Applied Catalysis B: Environmental 183 (2016) 407–416

Contents lists available at ScienceDirect

Applied Catalysis B: Environmental

journal homepage: www.elsevier.com/locate/apcatb

Decomposition of organic chemicals by zeolite-TiO_2 nanocomposite supported onto low density polyethylene film under UV-LED powered by solar radiation

Mohammad Reza Eskandarian [a,b], Mostafa Fazli [a,*,1], Mohammad Hossein Rasoulifard [c], Hyeok Choi [b,**,1]

[a] Department of Applied Chemistry, Faculty of Chemistry, Semnan University, Semnan 363-35196, Iran
[b] Department of Civil Engineering, The University of Texas at Arlington, Arlington, TX 76019-0308, United States
[c] Water & Wastewater Treatment Research Laboratory, Department of Chemistry, University of Zanjan, Zanjan 313-45195, Iran

ARTICLE INFO

Article history:
Received 16 July 2015
Received in revised form 5 October 2015
Accepted 6 November 2015
Available online 12 November 2015

Keywords:
TiO_2 photocatalysis
UV-LED
Photovoltaics
Persulfate
Zeolite

ABSTRACT

Zeolite-TiO_2 nanocomposite was synthesized to maximize its surface area for high reactivity and then immobilized onto a low density polyethylene film to enhance its mechanical stability and application practicality. Ultraviolet light emitting diode (UV-LED) was applied instead of traditional UV lamps to activate the TiO_2 composite. Photovoltaics was also introduced to utilize solar radiation as an energy source of UV-LED. The reactivity of zeolite-TiO_2 nanocomposite under UV-LED powered by solar radiation was evaluated in the presence of potassium persulfate ($K_2S_2O_8$) as an oxidant to decompose reactive dyes and pharmaceuticals (reactive black 5, cefiximetrihydrate, and phenazopyridine). Reactivity of various chemical, photolytic, photochemical, and photocatalytic decomposition processes and routes was in order of UV-LED ≈ TiO_2 ≈ zeolite ≈ zeolite-TiO_2 ≈ UV-LED/zeolite ≈ UV-LED/TiO_2 < $K_2S_2O_8$ « TiO_2/$K_2S_2O_8$ < zeolite-$K_2S_2O_8$ < UV-LED/$K_2S_2O_8$ < UV-LED/zeolite-TiO_2 < UV-LED/TiO_2/$K_2S_2O_8$ < UV-LED/zeolite/$K_2S_2O_8$ « zeolite-TiO_2/$K_2S_2O_8$ < UV-LED/zeolite-TiO_2/$K_2S_2O_8$. Use of zeolite-TiO_2 nanocomposite contributed to enhanced decomposition of target contaminants more significantly than any other factors such as addition of persulfate and introduction of UV-LED. Effect of persulfate concentration, absorbance spectral changes and discoloration, and reusability of zeolite-TiO_2 nanocomposite were also discussed. Since all devices including UV-LED were powered by a photovoltaic module and organic decomposition was successful, the photovoltaics-powered UV-LED photoreactor was proposed as a sustainable, self-powered, and practical point-of-use decontamination system to decompose water contaminants under solar radiation.

1. Introduction

Dyes are widely used in broad industrial sectors such as textile, leather tanning, cosmetics, paper, and food processing [1–5]. Reactive dyes used in textile industries are of particular concern due to their recalcitrance [6,7]. Physical (adsorption, membrane separation, and magnetic separation), chemical (electrochemical process, Fenton reaction, and ozonation), and biological methods (aerobic and anaerobic decomposition) have been applied for the treatment of dyes wastewater but their performance was not successful [8–12]. More recently, pharmaceuticals and personal care products (PPCPs) have been also found in many water resources and some of them are classified as emerging contaminants [13–17]. Various treatment methods, including coagulation–flocculation, biodegradation, biofiltration, ozonation, chemical precipitation, and adsorption, have been reported [18–22]. However, these conventional approaches showed low removal efficiency of PPCPs [23,24].

Advanced oxidation technologies based on generation of highly reactive radical species, which are in charge of chemical oxidation, have been suggested to be effective to decompose such recalcitrant organic chemicals [25]. In particular, titanium dioxide (TiO_2) photocatalysis is proven to generate hydroxyl radicals effectively under ultraviolet (UV) radiation [26,27]. Due to fast mass transfer, TiO_2 photocatalysts in aqueous suspension successfully decomposed

* Corresponding author. Fax: +98 231 333 8847.
** Corresponding author. Fax: + 1 817 272 2630.
E-mail addresses: mfazli@semnan.ac.ir (M. Fazli), hchoi@uta.edu (H. Choi).
[1] These authors contributed equally.

http://dx.doi.org/10.1016/j.apcatb.2015.11.004
0926-3373/

recalcitrant organic contaminants within reasonable time frame [28–31]. In spite of its high reactivity, suspension type of TiO_2 commonly requires a subsequent step for separation of TiO_2 particles after applications. To avoid the particle separation step, approaches to immobilize TiO_2 particles onto a substrate have been investigated [32]. However, immobilized type of TiO_2 suffers from slow mass transfer and thus needs much longer reaction time [33,34]. In addition, TiO_2 particles should stay attached firmly to a substrate under any circumstances. There is a need to develop a robust TiO_2/substrate composite with high catalytic surface area to reduce mass transfer limitation and with high mechanical stability to avoid catalyst detachment.

In addition to the challenge associated with particle immobilization, need of UV irradiation to TiO_2 is a huge hurdle. Conventional photocatalytic systems use traditional mercury lamps which show many disadvantages such as large size of lamps, low resistance to shock, high sensitivity to temperature, and most importantly danger of potential mercury release. Recently, studies have demonstrated use of light emitting diode (LED) to replace mercury lamps as a UV source, so-called UV-LED [35–39]. Advantages of UV-LED include high efficiency, low power consumption, wide functional temperature, long lifetime, no disposal problem, no warming-up time, and compactness [40,41]. UV-LED is also characterized with sustainability and recyclability [42,43]. Meanwhile, an economical, sustainable, affordable, and point-of-use decontamination route is increasingly needed when a TiO_2 photocatalytic system is applied for water treatment. Use of solar radiation is definitely one of solutions to the need (Fig. 1). Solar radiation has been used to produce UV for disinfection, photocatalysis, and many other applications [42]. In particular, photovoltaics can provide grid-independent energy [42,43]. Converting sustainable solar radiation to UV via photovoltaics is promising for photocatalytic water treatment.

This present study addresses the three major challenges explained above. First, a composite of TiO_2 (a known photocatalytic material with high reactivity) and zeolite (a known porous material with high surface area) was synthesized to maximize surface area for high reactivity. Then, the composite was immobilized onto a low density polyethylene (LDPE) film to enhance its mechanical stability and application practicality. Second, UV-LED was examined as an UV source to activate the TiO_2 composite. Third, photovoltaics was introduced to use solar radiation as an energy source of UV-LED. All devices in the photoreactor used in this study, including UV-LED, were also powered by the photovoltaic module.

Consequently, the objective of this study was to examine the reactivity of zeolite-TiO_2 nanocomposite supported onto LDPE film under UV-LED powered by solar radiation. The reactivity was measured with respect to decomposition of recalcitrant organic contaminants in water; reactive dyes and pharmaceuticals. Persulfate (i.e., peroxydisulfate) as a strong oxidant was also added to accelerate the decomposition reaction since persulfate is known to be decomposed under UV to generate sulfate radicals [44,45]. Accordingly, 16 different chemical, photolytic, photochemical, and photocatalytic systems were compared. The photovoltaics-powered UV-LED photoreactor with the novel zeolite-TiO_2 nanocomposite was proposed as a new sustainable, self-powered, and practical system to decompose water contaminants under solar radiation.

2. Experimental

2.1. Chemicals and materials

Three organic chemicals were chosen as target contaminants to decompose. Reactive black 5 (RB5) was obtained from Alvan Sabet (Iran) and used without further purification. RB5 is known as one of the most recalcitrant reactive dyes [8]. For PPCPs, cefixime (CFX) and phenazopyridine (PhP) were obtained from Sigma–Aldrich (Germany). CFX is an antibiotic for the treatment of bacterial infection. It is on the World Health Organization's list of essential medicines and thus CFX is found in many water resources [46,47]. PhP is commonly used as an analgesic drug in urinary tract treatment and many other medical prescriptions. Since PhP has an azo group, it is refractory. The molecular structure, chemical properties, and other characteristics of the target contaminants are given in Table S1. Potassium peroxydisulfate ($K_2S_2O_8$) purchased from Merck (Germany) was used as a persulfate source. Hydrochloric acid (HCl) and sodium hydroxide (NaOH) were obtained from Merck (Germany). Solutions of the chemicals were prepared just before their use to avoid change of their concentrations due to potential self-decomposition. Ethanol (C_2H_5OH) was purchased from Zakariya Razi (Iran). Double distilled water was utilized for all experiments (GFL, type 2008, Germany).

TiO_2 nanoparticles (Degussa P-25) with surface area of $55\,m^2\,g^{-1}$ and particle size of 30 nm were supplied by Fluka (Germany). LDPE film was provided by Iran Polymer and Petrochemical Institute (Iran). Natural zeolite was supplied by Mianeh Mine (Iran). Around 90 weight% of the zeolite contained clinoptilolite, which is composed of a microporous arrangement of silica and alumina tetrahedral with complex formula of $(Na,K,Ca)_{2-3}Al_3(Al,Si)_2Si_{13}O_{36}{\cdot}12H_2O$. Average size of the zeolite particles with surface area of $91\,m^2\,g^{-1}$ was 9.4 μm. Impurities in the zeolite such as Fe_2O_3, TiO_2, MnO, and P_2O_5 were reported elsewhere at 1.30%, 0.3%, 0.04%, and 0.01%, respectively [48].

2.2. Catalyst immobilization and characterization

To immobilize TiO_2 nanoparticles onto LDPE film, thermally-activated immobilization method was employed as described elsewhere [48,49]. Briefly, 0.5 g of TiO_2 nanoparticles were rigorously mixed with 15 mL of ethanol to make a homogeneous suspension for 12 h. LDPE film was cleaned with water and cut in 10 cm × 10 cm dimension. TiO_2 suspension was poured onto the surface of LDPE film. To avoid deformation of LDPE film during drying at 150 °C in an oven for 2 h, it was placed between two pieces of steel sheets. After cooling by natural air flow, it was washed with water several times to remove any un-immobilized TiO_2 particles. Result showed TiO_2 density on the film was at $3.5 \pm 0.1\,mg\,cm^{-2}$ (total 0.35 g per film). By following the exact same procedure, zeolite was immobilized onto LDPE film and zeolite density on the film was at $2.5 \pm 0.1\,mg\,cm^{-2}$ (total 0.25 g per film). Method for immobilization of zeolite-TiO_2 nanocomposite onto LDPE film was very similar to the approach mentioned above. In this case, 0.25 g of TiO_2 and 0.25 g of zeolite were mixed with 15 mL of ethanol. The solution was placed in an oven at 400 °C for 4 h. After calcination step followed by natural cooling, 15 mL of ethanol was added. The subsequent procedures for immobilization and drying were the same as above. Zeolite-TiO_2 density on the film was at $4.3 \pm 0.1\,m\,cm^{-2}$ (total 0.43 g per film).

The materials were characterized to identify their properties. Fourier transform infrared spectroscope (FT-IR, Nicolet, iS10, Thermo Scientific, US) was used to determine chemical bindings in the composites. Scanning electron microscope (SEM, TESCAN MIRA3-FEG, Czech Republic) was used to probe the morphology. Atomic force microscope (AFM, Dual scope/Raster scope C26, DME, Denmark) was utilized to examine the surface properties.

2.3. Photovoltaics and UV-LED setup

Photovoltaic module is a semiconductor device which converts solar energy into direct current. It was specially fabricated to provide energy to the particular UV-LED. The overall configuration of

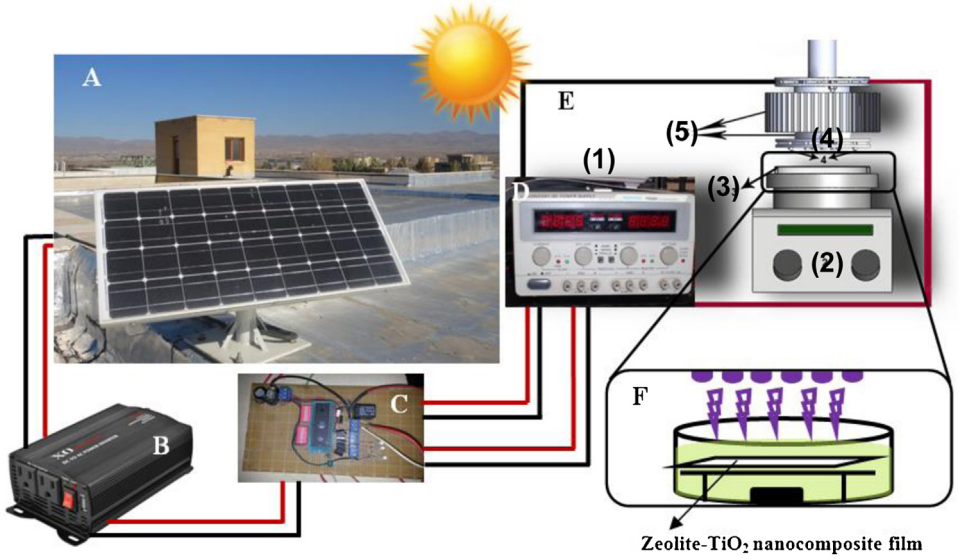

Fig. 1. Configuration of a photovoltaics-powered UV-LED photoreactor (A) solar panel, (B) direct current/alternating current converter, (C) regulator, (D) direct current-constant current power supply, (E) UV-LED photoreactor setup ((1) DC power supplier, (2) magnetic stir, (3) reactor, (4) UV-LED, and (5) heat sink system), and (F) TiO_2 photocatalytic reactor for decomposition of water contaminants. Please also note Fig. S1 for power storage and regulator safety box in the solar panel.

a photovoltaics/UV-LED photoreactor is shown in Fig. 1 (please also note Fig. S1). A polycrystalline solar panel (TN-P225-250, Energy Technology, China) with power range of 225–250 W and efficiency of 13.8–15.3% was used. All devices used in this photoreactor including UV-LED were powered by the photovoltaic module. An electrical inverter (TAXI-300W Model, Johsun Tech, China) was used to convert direct current to alternating current. To control electrical current, a regulator and a constant current power supply (KORAD KA3005D-3S, China) were applied. Six pieces of TO-18 UV-LED were obtained from Seoul Opto Device (South Korea) and power of each UV-LED was 3 W. A cooling system was attached to UV-LED. Current and voltage were adjusted by a direct current power supply with galvanostatic operational option. Spectrum of the emission wavelength of UV-LED was measured by an ultrafast fiber optic spectrometer (AvaSpec-128, Avantes, Netherlands). As shown in Fig. S2, the maximum emission wavelength was identified at 395 nm. Electrical current, forward voltage, optimum current were reported elsewhere [40,41].

2.4. Photocatalytic experiments

To test the effectiveness of the UV-LED photoreactor, decomposition of RB5, CFX, and PhP at 20 mg L^{-1} each or in a mixture (total 60 mg L^{-1}) was monitored. Various control, reference, and main experiments were set up, including self-decomposition (background), zeolite, TiO_2, zeolite-TiO_2, UV-LED, UV-LED/zeolite, UV-LED/TiO_2, and UV-LED/zeolite-TiO_2 (all materials were immobilized onto LDPE film). In each case, persulfate at 0–160 mM was added to accelerate decomposition of the target contaminants because persulfate is known to be decomposed under UV to generate sulfate radicals as strong as hydroxyl radicals [44,45].

A batch type photocatalytic reactor was set up. A 140 mm crystallizer (250 mL volume) with a magnet stirrer under a holder of LDPE film was used. Reaction volume was at 100 mL. One LDPE film coated with each material was added to the reactor, giving 0.25 g of zeolite, 0.35 g of TiO_2, or 0.43 g of zeolite-TiO_2. The initial pH of reaction solution was adjusted at 7.0 by adding HCl or NaOH and no buffer solution was used to avoid any complexity (changes of solution pH during reaction were not significant). The solution in the crystallizer was stirred continuously. Six UV-LEDs (with 3 W each) were turned on at room temperature (25 ± 2 °C). Sampling was done at each 5 min interval. Concentrations of RB5, CFX, and PhP were measured by a UV–vis spectrophotometer (Shimadzu UV-160, Japan) at λ_{max} = 596 nm, 436 nm, and 288 nm, respectively. In this specific case, there was no obvious conflict of UV–vis wavelength absorbance among the chemicals. The reusability of zeolite-TiO_2 composite was evaluated by repeating the batch test. After each cycle, used zeolite-TiO_2 nanocomposite was washed and cleaned with water and dried for next cycle.

3. Results and discussion

3.1. Properties of zeolite-TiO_2 nanocomposite

Immobilized zeolite, TiO_2, and zeolite-TiO_2 composite onto LDPE film were used for all experiments and materials characterization (e.g., TiO_2 later denotes TiO_2 immobilized onto LDPE film). LDPE was chosen because of many advantages such as low cost, light weight, compatibility with other materials, flexibility in shape forming, and high application potential. LDPE is not degraded by UV-A irradiation. Its decomposition is less likely to occur during the chemical reactions in this study, considering the low intensity and long wavelength of UV-LED. In fact, many studies have demonstrated use of polymeric materials as a substrate for TiO_2 immobilization (i.e., TiO_2 photocatalytic polymeric membranes) [50].

FT-IR analysis was used to investigate the chemical structures of LDPE film and composite, as shown in Fig. 2. FTIR spectra of LDPE shown in Fig. 2(a) did not make any conflict with FTIR spectra of the other materials. Fig. 2(b) and (c) well represented zeolite and TiO_2, respectively. Changes in FTIR spectra of zeolite-TiO_2 composite shown in Fig. 2(d) were obvious. A band in region of 3391.50 cm^{-1} was related to tensional vibration of hydroxyl groups in zeolite and a corresponding flexural vibration band was clearly visible in region of 1640.08 cm^{-1}. Those peaks were shifted to 3446.58 cm^{-1} and 1626.73 cm^{-1} for zeolite-TiO_2. In addition, a flexural vibration band for Ti-O in TiO_2 was observed at 1066.79 cm^{-1}. The peak was shifted to 1019.22 cm^{-1} for zeolite-TiO_2. These imply certain chemical interactions between zeolite and TiO_2. The peaks shown in each of zeolite and TiO_2 were also generally observed in zeolite-TiO_2 composite, implying no significant changes in the basic chemical structures of zeolite and TiO_2. As a result, zeolite-TiO_2 composite

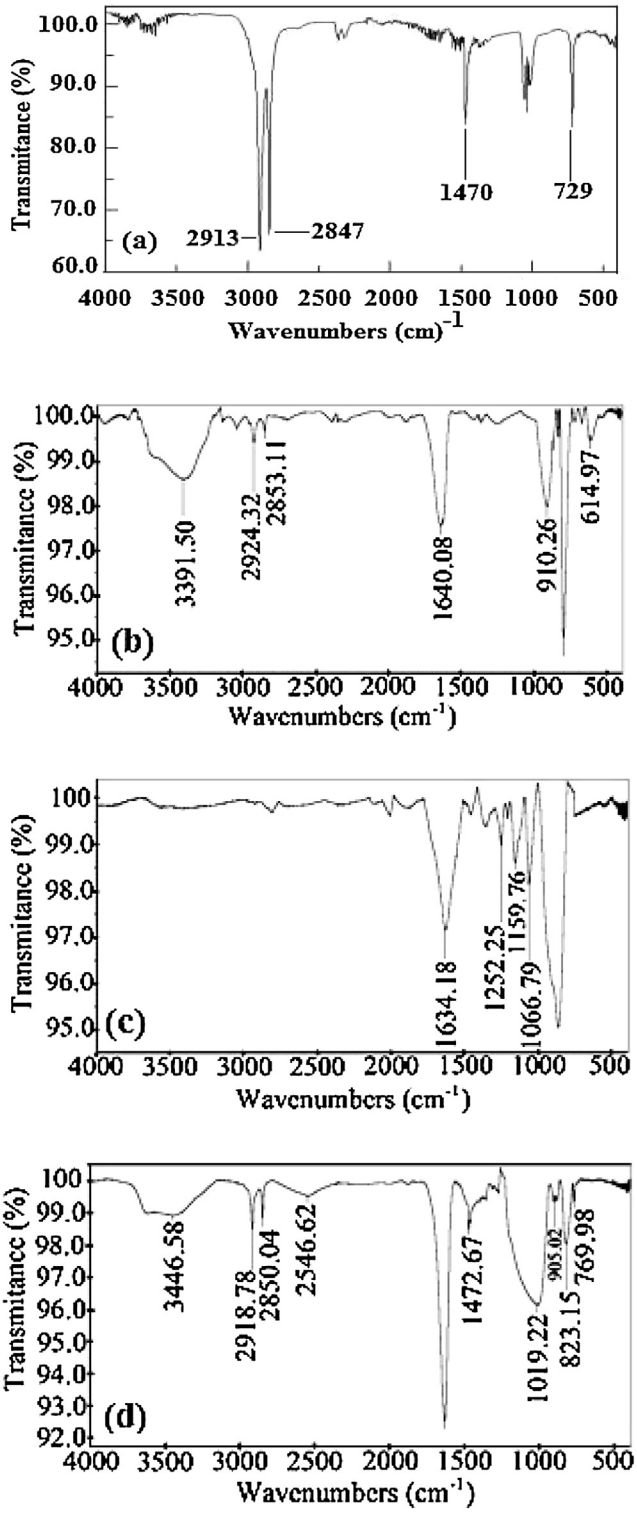

Fig. 2. FT-IR spectra of (a) LDPE (b) zeolite, (c) TiO_2, and (d) zeolite-TiO_2 nanocomposite. All materials were immobilized onto LDPE film.

was expected to show the photocatalytic activity of TiO_2 as well as the adsorption capability of zeolite.

SEM images of the materials are shown in Fig. 3. Fig. 3(a) shows SEM image of LDPE film. In comparison to TiO_2 shown in Fig. 3(b) and (c), zeolite-TiO_2 composite shown in Fig. 3(d)–(f) exhibited interesting morphology. Uniform size of TiO_2 nanoparticles at around 30 nm and highly porous structure originated from interparticle space were clearly observed. The result supports the positive effect of zeolite on dispersion and immobilization of TiO_2 particles. The highly porous nature of zeolite-TiO_2 composite might have high potential for enhanced reactivity.

AFM was utilized to investigate the morphology of the materials, as shown in Fig. 4. When comparing LDPE shown in Fig. 4(a) with TiO_2 shown in Fig. 4(b) and (c), it was noted that LDPE film was uniformly coated with TiO_2 nanoparticles. The 3D topography and phase diagram of TiO_2 are shown in Fig. 4(d) and (e), respectively.

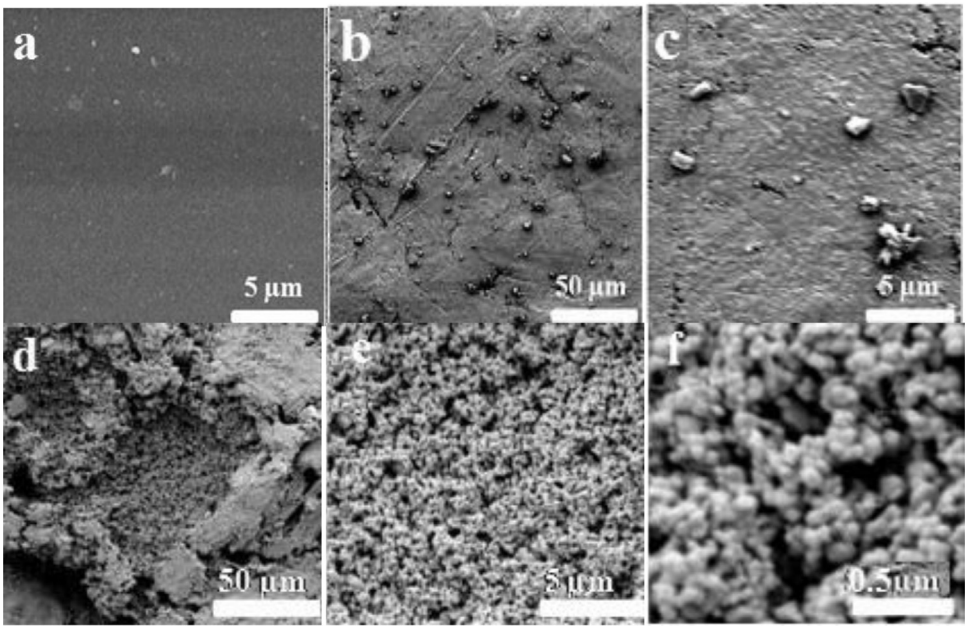

Fig. 3. SEM images of (a) LDPE, (b) and (c) LDPE coated with TiO_2, and (d)–(f) LDPE coated with zeolite-TiO_2 nanocomposite.

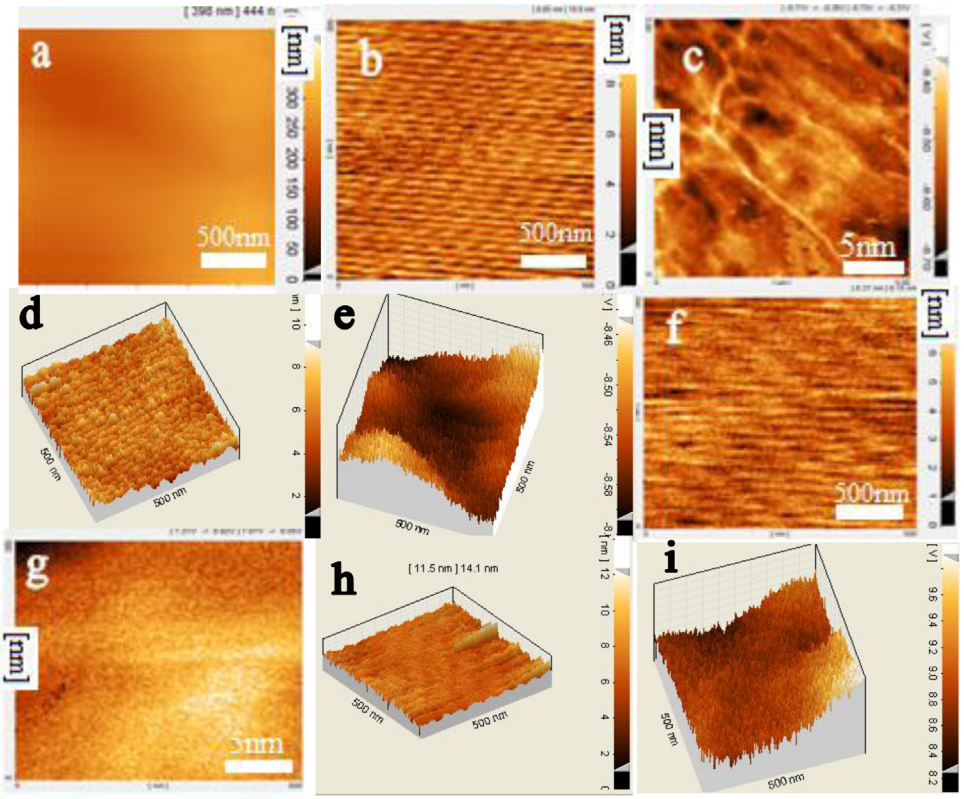

Fig. 4. AFM images of (a) LDPE, (b) and (c) LDPE coated with TiO_2 ((b) at 500 nm and (c) at 5 nm), (d) 3D topography of LDPE coated with TiO_2, (e) 3D phase diagram of LDPE coated with TiO_2, (f) and (g) LDPE coated with zeolite-TiO_2 nanocomposite ((f) at 500 nm and (g) at 5 nm), (h) 3D topography of LDPE coated with zeolite-TiO_2 nanocomposite, and (i) 3D phase diagram of LDPE coated with zeolite-TiO_2 nanocomposite.

Areas with lighter colors are related to background material (i.e., LDPE film) while those with darker colors represent immobilized TiO_2 particles. In general, TiO_2 particles were well distributed onto the film while some areas such as troughs in the film had much higher TiO_2 density. The same analysis was conducted for zeolite-TiO_2 composite, as shown in Fig. 4(f)–(i). Comparison between TiO_2 shown in Fig. 4(b) and (c) and zeolite-TiO_2 shown in Fig. 4(f) and (g) clearly indicated that TiO_2 particles were more uniformly immobilized onto LDPE film in the presence of zeolite. The finding was further supported by Fig. 3(h) and (i). The surface roughness indicating uniformity of surface was calculated at 8.5–11 nm for TiO_2 and 5.5–7.2 nm for zeolite-TiO_2. Surface roughness was greatly improved by introducing zeolite.

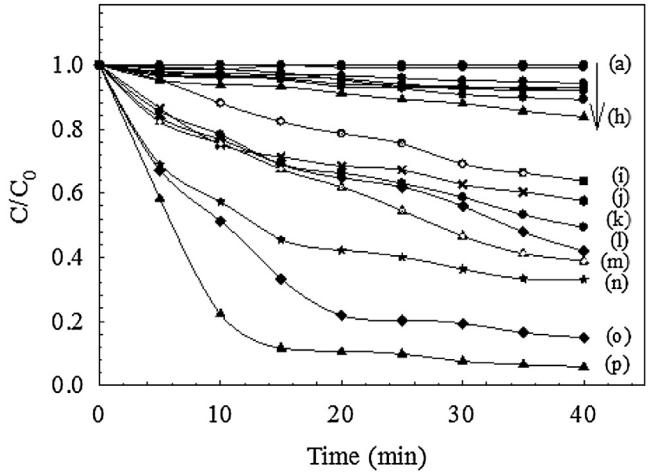

Fig. 5. Reactivity of various photochemical processes and routes with respect to decomposition of a mixture of RB5, CFX, and PhP: (a) control (b) UV-LED, (c) TiO_2, (d) zeolite, (e) zeolite-TiO_2, (f) UV-LED/zeolite, (g) UV-LED/TiO_2, (h) $K_2S_2O_8$, (i) $TiO_2/K_2S_2O_8$, (j) zeolite/$K_2S_2O_8$, (k) UV-LED/$K_2S_2O_8$, (l) UV-LED/zeolite-TiO_2, (m) UV-LED/$TiO_2/K_2S_2O_8$, (n) UV-LED/zeolite/$K_2S_2O_8$, (o) zeolite-$TiO_2/K_2S_2O_8$, and (p) UV-LED/zeolite-$TiO_2/K_2S_2O_8$, (I = 1.40 A, UV-LED = 18 W, pH neutral at 7.0 (no buffer), $[K_2S_2O_8]_0$ = 80 mM, $[RB5]_0 = [CFX]_0 = [PhP]_0$ = 20 mg L^{-1}).

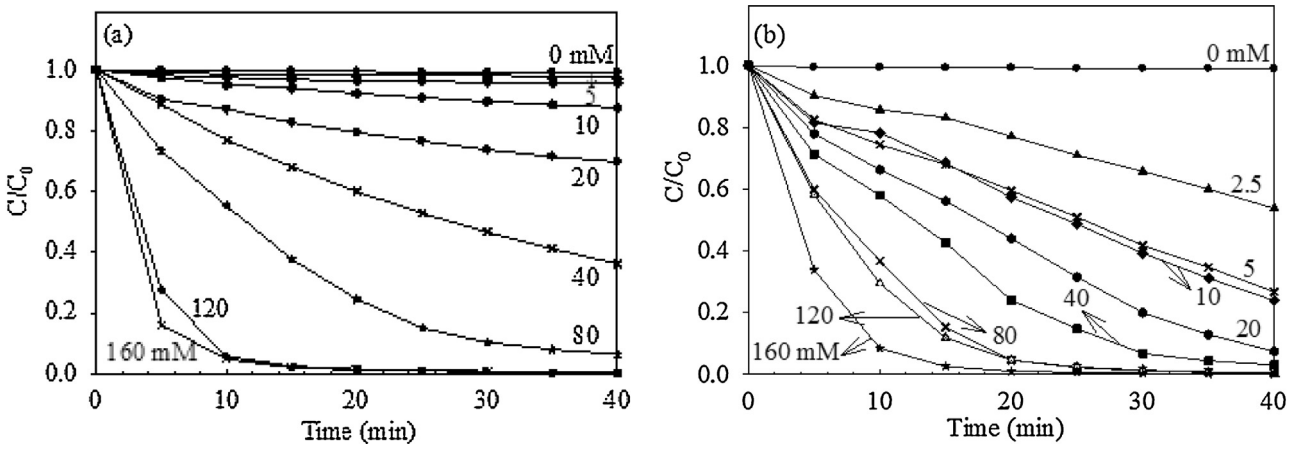

Fig. 6. Effect of persulfate concentration at 0–160 mM on decomposition of RB5 in case of (a) UV-LED and (b) UV-LED and zeolite-TiO_2 nanocomposite (I = 1.40 A, UV-LED = 18 W, pH neutral at 7.0 (no buffer), $[RB5]_0$ = 20 mg L^{-1}).

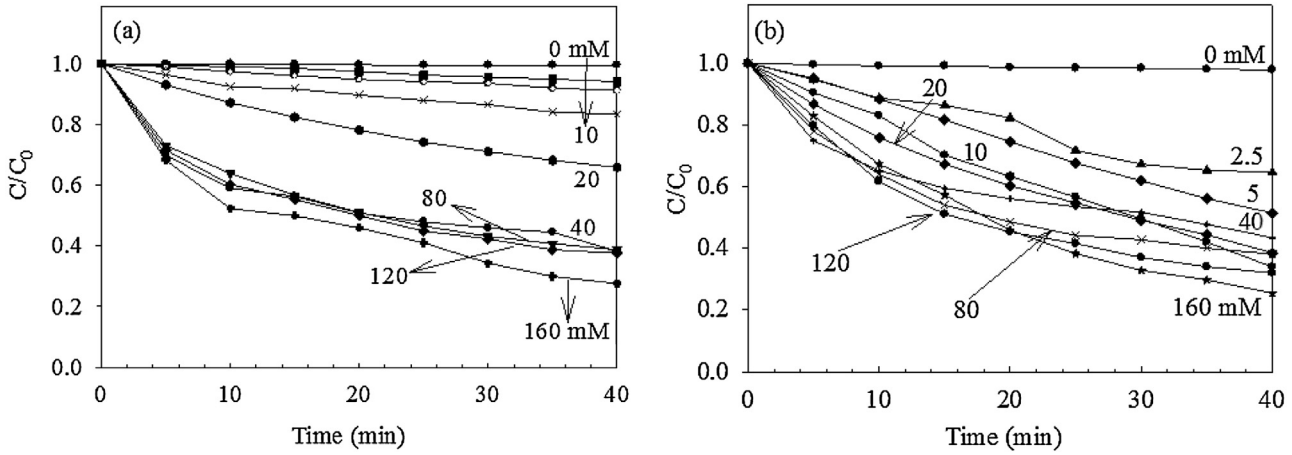

Fig. 7. Effect of persulfate concentration at 0–160 mM on decomposition of CFX in case of (a) UV-LED and (b) UV-LED and zeolite-TiO_2 nanocomposite (I = 1.40 A, UV-LED = 18 W, pH neutral at 7.0 (no buffer), $[CFX]_0$ = 20 mg L^{-1}).

3.2. Comparison of various decomposition routes

As shown in Fig. 5, various control, reference, and main experiments were set up to decompose a mixture of RB5, CFX, and PhP, including self-decomposition, zeolite, TiO_2, zeolite-TiO_2, UV-LED, UV-LED/zeolite, UV-LED/TiO_2, and UV-LED/zeolite-TiO_2 in the absence and presence of persulfate (total 16 conditions). It should

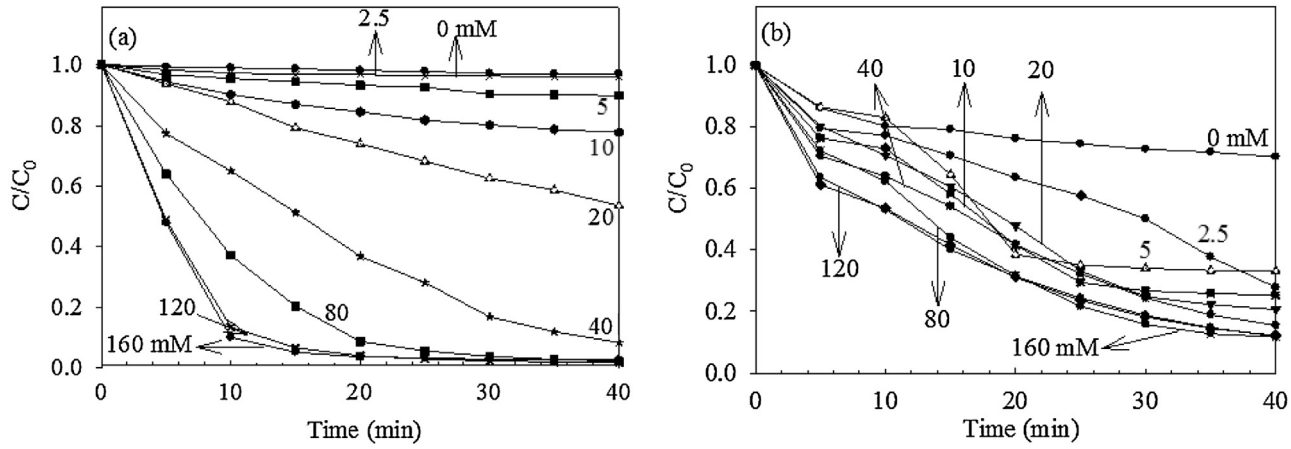

Fig. 8. Effect of persulfate concentration at 0–160 mM on decomposition of PhP in case of (a) UV-LED and (b) UV-LED and zeolite-TiO_2 nanocomposite (I = 1.40 A, UV-LED = 18 W, pH neutral at 7.0 (no buffer), $[PhP]_0$ = 20 mg L^{-1}).

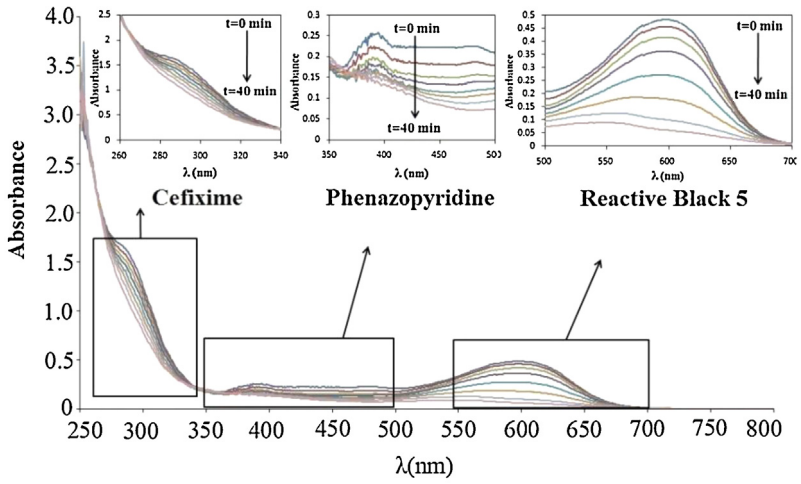

Fig. 9. Spectral change during decomposition of a mixture of RB5, CFX, and PhP by using zeolite-TiO_2 nanocomposite under UV-LED in the presence of persulfate (I = 1.40 A, UV-LED = 18 W, T = 25 °C, pH neutral at 7.0 (no buffer), $[K_2S_2O_8]_0$ = 80 mM, $[RB5]_0 = [CFX]_0 = [PhP]_0$ = 20 mg L^{-1}).

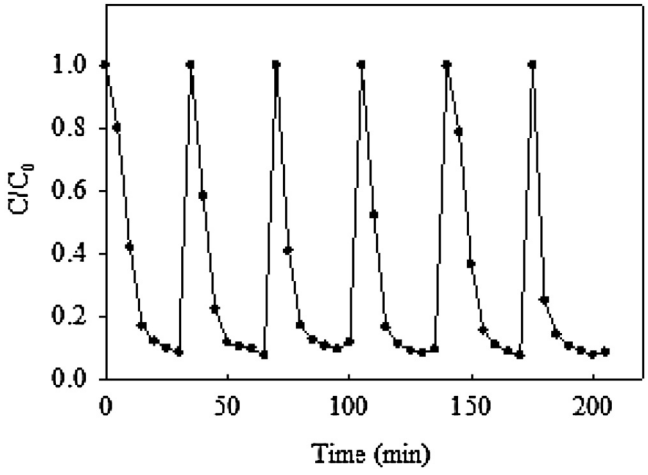

Fig. 10. Reactivity change of zeolite-TiO_2 nanocomposite upon repeated use (6 cycles) with respect to decomposition of a mixture of RB5, CFX, and PhP (I = 1.40 A, UV-LED = 18 W, T = 25 °C, pH neutral at 7.0 (no buffer), $[K_2S_2O_8]_0$ = 80 mM, $[RB5]_0 = [CFX]_0 = [PhP]_0$ = 20 mg L^{-1}).

be noted that less attention was given to understanding of reaction mechanisms, such as radical generation and identification, because the reaction mechanism in each system has been well understood [44,45,51–54]. Rather, the reactivity of the various decomposition routes was compared.

No self-decomposition of the contaminants was observed (Fig. 5(a)) and no direct photolysis of the contaminants by UV-LED

was also seen (Fig. 5(b)) because the contaminants are recalcitrant. Either TiO_2 (Fig. 5(c)), zeolite (Fig. 5(d)), or zeolite-TiO_2 (Fig. 5(e)) alone without UV-LED did not have any noticeable reactivity. Zeolite with UV-LED (Fig. 5(f)) also showed negligible reactivity. Those results were well expected, considering the nature of the materials. TiO_2 under UV-LED (Fig. 5(g)) also exhibited very low reactivity. In general, significant reactivity of a TiO_2/UV system is expected because hydroxyl radicals are known to be effectively generated [51,52]. This is particularly true only if UV intensity (power) is high enough and UV wavelength is short enough. However, solar radiation was used in this study to provide power to UV-LED, resulting in low UV intensity. In addition, UV wavelength from UV-LED (λ_{max} = 395 nm, note Fig. S2) is much longer than that from conventional mercury lamps (λ_{max} = 365 nm). The low reactivity might also be related to mass transfer limitation of the contaminants to the nonporous TiO_2, P-25.

Persulfate as a strong oxidant (Fig. 5(h)) showed some reactivity towards the contaminants but decomposition kinetics was too slow. This result supports conventional chemical oxidation processes do not work effectively for the decomposition of recalcitrant contaminants such as reactive dyes and PPCPs. Interestingly, addition of persulfate to TiO_2 (Fig. 5(i)) or zeolite (Fig. 5(j)) improved decomposition kinetics. There have been no reports that either TiO_2 or zeolite activates persulfate. Since persulfate is well known to be activated by transition metals (e.g., iron, copper, and cobalt) to generate sulfate radicals as a strong oxidant, transition metals as impurities present in zeolite and TiO_2 may have activated persulfate to trigger the Fenton-like reaction (e.g., the zeolite used in this study contains Fe_2O_3 at 1.3%) [48,53,54]. Anipsitakis and Dionysiou reported that persulfate conjugated with transition metals at levels of a few mg L^{-1} demonstrated significant reactivity towards the transformation of 2,4-dichlorophenol [53].

Persulfate under UV-LED demonstrated successful decomposition of the contaminats (Fig. 5(k)). Photolysis of persulfate by UV is well known to produce sulfate radicals [44,45]. Compared to negligible reactivity of zeolite with UV-LED (Fig. 5(f)) and TiO_2 with UV-LED (Fig. 5(g)), zeolite-TiO_2 composite with UV-LED (Fig. 5(l)) exhibited significant reactivity. This is because introduction of zeolite greatly improved TiO_2 particle dispersion, film uniformity, and surface area, as investigated in the previous section. Decomposition by $TiO_2/K_2S_2O_8$ (Fig. 5(i)) and zeolite/$K_2S_2O_8$ (Fig. 5(j)) was further enhanced by introduction of UV-LED (Fig. 5(m) and Fig. 5(n), respectively) due to generation of hydroxyl radicals from TiO_2/UV-LED and/or sulfate radicals from persulfate/UV-LED [44,45,51–54]. In comparison to $TiO_2/K_2S_2O_8$ (Fig. 5(i)) or zeolite/$K_2S_2O_8$ (Fig. 5(j)), use of zeolite-TiO_2 composite in conjugation with persulfate (Fig. 5(o)) showed much significant reactivity. This result in agreement with the result in Fig. 5(l) suggests zeolite-TiO_2 composite is promising in the presence of either UV-LED or persulfate, compared to zeolite or TiO_2 alone.

In particular, zeolite-TiO_2 under UV-LED in the presence of persulfate (Fig. 5(p)), which attacked the contaminants via various chemical, photolytic, photochemical, and photocatalytic routes in combination, showed best decomposition kinetics. Most of the recalcitrant contaminants were decomposed immediately within 10 min. Considering initial high concentration of the contaminants at 60 mg L^{-1}, the reactivity is encouraging. In summary, the reactivity of the various decomposition processes and routes was in order of UV-LED ≈ TiO_2 ≈ zeolite ≈ zeolite-TiO_2 ≈ UV-LED/zeolite ≈ UV-LED/TiO_2 < $K_2S_2O_8$ « $TiO_2/K_2S_2O_8$ < zeolite/$K_2S_2O_8$ < UV-LED/$K_2S_2O_8$ < UV-LED/zeolite-TiO_2 < UV-LED/$TiO_2/K_2S_2O_8$ < UV-LED/zeolite/$K_2S_2O_8$ « zeolite-$TiO_2/K_2S_2O_8$ < UV-LED/zeolite-$TiO_2/K_2S_2O_8$. Use of zeolite-TiO_2 contributed to the enhanced decomposition of the contaminants more significantly than any other factors such as addition of persulfate and introduction of UV-LED.

3.3. Impacts of zeolite-TiO_2 and persulfate concentration

Previously, zeolite-TiO_2 composite enhanced the decomposition of the target contaminants in mixture. Consequently, the impact of zeolite-TiO_2 composite under UV-LED on the decomposition of individual target contaminant was investigated while the effect of persulfate concentration was also evaluated, as shown in Figs. 6–8. In particular, Figs. 6–8(a) shows results on UV-LED/$K_2S_2O_8$ systems for generation of sulfate radicals while Figs. 6–8(b) shows UV-LED/zeolite-$TiO_2/K_2S_2O_8$ systems for generation of sulfate radicals and hydroxyl radicals [51–54].

Fig. 6(a) shows decomposition of RB5 by different concentrations of persulfate under UV-LED. When persulfate was added, RB5 was successfully decomposed due to sulfate radical generation via persulfate decomposition under UV-LED [53,54]. In this case, mechanism for the successful RB5 decomposition is dominantly sulfate radical oxidation because there was no photolysis of RB5 by UV-LED in the absence of persulfate (note 0 mM of persulfate in Fig. 6(a)) and persulfate alone even at 80 mM did not show significant reactivity (note Fig. 5(h)). At persulfate concentrations of more than 120 mM, almost complete decomposition of RB5 was observed. Fig. 6(b) shows decomposition of RB5 by different concentrations of persulfate under UV-LED in the presence of zeolite-TiO_2 composite. The similar trend to the previous UV-LED/$K_2S_2O_8$ system (Fig. 6(a)) was observed. However, decomposition of RB5 was greatly improved in the presence of zeolite-TiO_2 composite. Decomposition kinetics at 5 mM of persulfate under UV-LED conjugated with zeolite-TiO_2 was equivalent to that at 40 mM of persulfate under UV-LED without zeolite-TiO_2.

As proven in Fig. 5(e), zeolite-TiO_2 alone did not remove RB5 because of negligible adsorption of RB5. As a result, the enhanced decomposition shown in Fig. 6(b), compared to Fig. 6(a), can be attributed to generation of hydroxyl radicals from zeolite-TiO_2 under UV-LED [55]. Consequently, the UV-LED/zeolite-$TiO_2/K_2S_2O_8$ system generates both hydroxyl radicals from UV-LED/zeolite-TiO_2 and sulfate radicals from UV-LED/$K_2S_2O_8$, implying the highest reactivity. In addition, persulfate might also react with electrons in the conduction band of TiO_2 and thus generate other reactive species [56,57]. Interestingly, the enhanced decomposition of RB5 by zeolite-TiO_2 was observed only at persulfate concentrations of up to 80 mM while it was not observed at higher persulfate concentrations (i.e., 120 mM and 160 mM). In other words, introduction of zeolite-TiO_2 to the system for the generation of hydroxyl radicals is meaningless when persulfate concentration is high enough. Excessive amount of sulfate radicals are generated fast and homogeneously by persulfate at such high concentrations under UV-LED and promptly attack RB5 while hydroxyl radicals are generated relatively slowly and heterogeneously by zeolite-TiO_2 under UV-LED. In nature, decomposition of RB5 heavily relies on sulfate radical mechanism. This can explain the negligible difference in RB decomposition kinetics between UV-LED/$K_2S_2O_8$ and UV-LED/zeolite-$TiO_2/K_2S_2O_8$ at high persulfate concentrations.

CFX and PhP (Figs. 7 and 8) showed similar trends to RB5, with respect to effects of the presence of zeolite-TiO_2 and concentration of persulfate. Photocatalytic decomposition of PhP by zeolite-TiO_2 under UV-LED in the absence of persulfate was observed. One unexpected result was also shown for PhP (Fig. 8). At lower concentrations of persulfate, the presence of zeolite-TiO_2 greatly improved decomposition of PhP as observed consistently for the other contaminants while at concentrations of persulfate more than 40 mM, the presence of zeolite-TiO_2 rather inhibited decomposition of PhP (more or less similar result was also observed for RB5 under per-

sulfate concentrations more than 120 mM and 160 mM (Fig. 6)). Adverse effect of excessive amount of an oxidant and/or a catalyst on radical generation has been often reported (in-depth study is needed in future) [58,59]. At too high concentrations of hydroxyl radicals, their self-conjugation occurs to transform to less reactive species. An oxidizing chemical at concentrations higher than optimum concentration can act as a hole or a radical scavenger and react with TiO_2 to form less reactive intermediates such as peroxy [60]. Comparing decomposition kinetics of the contaminants, CFX containing more azo and diazo groups and three stubborn rings in its structure was the most recalcitrant, followed by PhP and RB 5 (Table S1) [46,47].

3.4. Spectral changes and discoloration

Representative absorbance spectral changes for a mixture of RB5, CFX, and PhP are shown in Fig. 9. CFX is colorless. Upon increases in reaction time and persulfate concentration, the absorbance peaks for all contaminants were faded out. Color removal over time was also visually observable (Fig. S3). Spectral changes indicated that all azo and diazo bonds were broken after 40 min mainly because nitrogen–nitrogen bonds are most vulnerable to attack by the radicals. Decomposition of RB5 based on the spectral absorbance change was much faster than CFX and PhP, which is in agreement with the results observed in Figs. 6–8.

3.5. Reusability of zeolite-TiO_2 nanocomposite

Reusability of zeolite-TiO_2 composite was briefly assessed, as shown in Fig. 10. Reusability is important for full scale commercialization and application of the material to industrial water and wastewater treatment. The experiment was conducted under standard conditions (neutral pH, 80 mM of persulfate, mixture of three contaminants at 60 mg L^{-1} (each 20 mg L^{-1}), zeolite-TiO_2, and UV-LED). Once pseudo steady state decomposition was achieved, LDPE film coated with zeolite-TiO_2 was recovered, cleaned with water, and dried naturally. This procedure was repeated for 6 cycles. Consistent decomposition kinetics was observed over cycles, implying zeolite-TiO_2 was firmly attached to LDPE film and thus not lost in each cycle and zeolite-TiO_2 also did not seem to be deactivated (i.e., no significant fouling).

4. Conclusions

Zeolite-TiO_2 nanocomposite immobilized onto LDPE film showed improved properties such as uniform TiO_2 dispersion and high surface area. Its reactivity under UV-LED powered by solar radiation was evaluated in the presence of persulfate. Reactivity of various decomposition processes and routes was in order of UV-LED ≈ TiO_2 ≈ zeolite ≈ zeolite-TiO_2 ≈ UV-LED/zeolite ≈ UV-LED/TiO_2 < $K_2S_2O_8$ « $TiO_2/K_2S_2O_8$ < zeolite/$K_2S_2O_8$ < UV-LED/$K_2S_2O_8$ < UV-LED/zeolite-TiO_2 < UV-LED/$TiO_2/K_2S_2O_8$ < UV-LED/zeolite/$K_2S_2O_8$ « zeolite $TiO_2/K_2S_2O_8$ < UV-LED/zeolite-$TiO_2/K_2S_2O_8$. Use of zeolite-TiO_2 composite contributed to the enhanced decomposition of reactive dyes and pharmaceuticals more significantly than any other factors such as addition of persulfate and introduction of UV-LED. Sulfate radicals generated from persulfate under UV-LED decomposed contaminants successfully. Enhanced decomposition by generation of additional hydroxyl radicals by zeolite-TiO_2 under UV-LED was also observed only at persulfate concentrations lower than 80 mM. Since all devices including UV-LED were powered by the photovoltaic module; organic decomposition was enhanced; and zeolite-TiO_2 composite was proven to be reusable, the photovoltaics-powered UV-LED photoreactor with zolite-TiO_2 nanocomposite was proposed as a sustainable, self-powered, and practical point-of-use decontamination system to decompose water contaminants under solar radiation.

Acknowledgements

This research was supported in part by the Texas Higher Education Coordinating Board through the Norman Hackerman Advanced Research Program (THECB13311). The Iran Ministry of Science, Research, and Technology supported Eskandarian via the visiting research program.

Appendix A. Supplementary data

Supplementary data associated with this article can be found, in the online version, at http://dx.doi.org/10.1016/j.apcatb.2015.11.004.

References

[1] C.I. Pearce, J.R. Lloyd, J.T. Guthrie, Dyes Pigments 58 (2003) 179–196.
[2] G. McMullan, C. Meehan, A. Conneely, N. Kirby, T. Robinson, P. Nigam, I.M. Banat, R. Marchant, W.F. Smyth, Appl. Microbiol. Biotechnol. 56 (2001) 81–87.
[3] G. Moussavi, M. Mahmoudi, J. Hazard. Mater. 168 (2009) 806–812.
[4] R.M. Christie, Environmental Aspects of Textile Dyeing, Woodhead, Boca Raton, Cambridge, 2007.
[5] X. Yang, B. Al-Duri, Chem. Eng. J. 83 (2001) 15–23.
[6] T.O. Mahony, E. Guibal, J. Tobin, Enzyme Microbiol. Technol. 31 (2002) 456–463.
[7] K.Z. Elwakeel, M. Rekaby, J. Hazard. Mater. 188 (2011) 10–18.
[8] Z. Atafar, A. Mesdaghinia, J. Nouri, M. Homaee, M. Yunesian, Environ. Monitor. Assess. 160 (2010) 83–89.
[9] G.M. Nabil, N.M. El-Mallah, M.E. Mahmoud, J. Ind. Eng. Chem. 20 (2014) 994–1002.
[10] M. Fathinia, A.R. Khataee, J. Ind. Eng. Chem. 19 (2013) 1525–1534.
[11] C. Allegre, P. Moulin, M. Maisseu, F. Charbit, J. Membr. Sci. 269 (2006) 15–34.
[12] K. Ranganathan, K. Karunagaran, D.C. Sharma, Resour. Conserv. Recycl. 50 (2007) 306–318.
[13] Z. Hasan, J. Jeon, S.H. Jhung, J. Hazard. Mater. 209–210 (2012) 151–157.
[14] T. Heberer, Toxicol. Lett. 131 (2002) 5–17.
[15] H. Tungudomwongsa, J. Leckie, T. Mill, J. Adv. Oxid. Technol. 9 (2006) 59–64.
[16] S.M. Rivera-Jimenez, A.J. Hernandez-Maldonado, Micropor. Mesopor. Mat. 116 (2008) 246–252.
[17] T.A. Ternes, J. Stuber, N. Herrmann, D. McDowell, A. Ried, M. Kampmann, B. Teiser, Water Res. 37 (2003) 1976–1982.
[18] G.R. Boyda, H. Reemtsmaa, D.A. Grimmb, S. Mitrac, Sci. Total Environ. 311 (2003) 135–149.
[19] A. Joss, S. Zabczynski, A. Gobel, B. Hoffmann, D. Loffler, C.S. McArdell, T.A. Ternes, A. Thomsen, H. Siegrist, Water Res. 40 (2006) 1686–1696.
[20] V. Matamorosa, C. Ariasb, H. Brixb, J.M. Bayonaa, Water Res. 43 (2009) 55–62.
[21] A. Lindstrom, I.J. Buerge, T. Poiger, P.A. Bergqvist, M.D. Muller, H.R. Buser, Environ. Sci. Technol. 36 (2002) 2322–2329.
[22] M. Ben Jaber, B. Anet, A. Amrane, C. Couriol, T. Lendormi, P. Le Cloirec, G. Cogny, R. Fillieres, Chem. Eng. J. 258 (2014) 420–426.
[23] M. Khraisheh, J. Kim, L. Campos, A.H. Al-Muhtaseb, A. Al-Hawari, M. Al Ghouti, G.M. Walker, J. Ind. Eng. Chem. 20 (2014) 979–987.
[24] V.K. Gupta, Suhas, J. Environ. Manage. 90 (2009) 2313–2342.
[25] K. Ikehata, N. Jodeiri Naghashkar, M. Gamal El-Din, Ozone Sci. Eng. 28 (2006) 353–414.
[26] X. Yan, R. Bao, S. Yu, Q. Li, Q. Jing, Russ. J. Phys. Chem. 86 (2012) 1479–1485.
[27] Q. Xiang, J. Yu, P.K. Wong, J. Colloid. Interf. Sci. 357 (2011) 163–167.
[28] P. Boule, D. Bahnemann, Environmental Photochemistry, Springer, Berlin, 1999.
[29] J.A. Byrne, B.R. Eggins, N.M.D. Brown, B. McKinney, M. Rouse, Appl. Catal. B: Environ. 17 (1998) 25–36.
[30] H. Lachhed, E. Puzenat, A. Houas, M. Ksibi, E. Elaloui, C. Guillard, J.H. Herrmann, Appl. Catal. B: Environ. 39 (2002) 75–90.
[31] K. VenkataSubba Rao, M. Subrahmanyam, P. Boule, Appl. Catal. B: Environ. 49 (2004) 239–249.
[32] A.Y. Shan, T.I. Mohd Ghazi, S. Abdul Rashid, Appl. Catal. A. 389 (2010) 1–8.
[33] J. Close, J. Ip, K.H. Lam, Renew. Energy 31 (2006) 1657–1664.
[34] A. Hamamoto, M. Mori, A. Takahashi, M. Nakano, N. Wakikawa, M. Akutagawa, T. Ikehara, Y. Nakaya, Y. Kinouchi, J. Appl. Microbiol. 103 (2007) 2291–2298.
[35] S. Vilhunen, H. Sarkka, M. Sillanpaa, Environ. Sci. Pollut. Res. 16 (2009) 439–442.
[36] A.C. Chevremont, A.M. Farnet, M. Sergent, B. Coulomb, J.L. Boudenne, Desalination 285 (2012) 219–225.
[37] A.C. Chevremont, A.M. Farnet, M. Sergent, B. Coulomb, J.L. Boudenne, Sci. Total Environ. 426 (2012) 304–310.

[38] M.A. Würtele, T. Kolbe, M. Lipsz, A. Külberg, M. Weyers, M. Kneissl, M. Jekel, Water Res. 45 (2011) 1481–1489.
[39] W.K. Jo, R.J. Tayade, Ind. Eng. Chem. Res. 53 (2014) 2073–2084.
[40] M.H. Rasoulifard, M. Fazli, M.R. Eskandarian, J. Ind. Eng. Chem. 20 (2014) 3695–3702.
[41] M.H. Rasoulifard, M. Fazli, M.R. Eskandarian, J. Ind. Eng. Chem. 24 (2015) 121–126.
[42] G.Y. Lui, D. Roser, R. Corkish, N. Ashbolt, P. Jagals, R. Stuetz, Sci. Total Environ. 493 (2014) 185–196.
[43] B. Parida, S. Iniyan, R. Goic, Renew. Sust. Energy Rev. 15 (2011) 1625–1636.
[44] J. Criquet, N.K. Leitner, Chemosphere 77 (2009) 194–200.
[45] M. Klapper, T. Brand, M. Steenbock, K. Mullen, ACS Symp. Ser. 768 (2000) 152–166.
[46] S.N.H. Azmi, B. Iqbal, N.S.H. Al-Humaimi, I.R.S. Al-Salmani, N.A.S. Al-Ghafri, N. Rahman, J. Pharm. Biomed. 3 (2013) 248–256.
[47] A. Mills, S.K. Lee, J. Photochem. Photobiol. A. 152 (2002) 233–247.
[48] S. Jalali Farahani, M. Nikazar, K. Keynejad, The 5th Environmental Engineering Annual Conference and Exhibition, Tehran, Iran, pp. 39–84, 2011.
[49] S. Izadyar, S. Fatemi, Ind. Eng. Chem. Res. 52 (2013) 10961–10968.
[50] X.W. Zhang, D.K. Wang, J.C.D. da Costa, Catal. Today 230 (2014) 47–54.
[51] M.R. Hoffmann, S.T. Martin, W. Choi, D.W. Bahnemann, Chem. Rev. 95 (1995) 69–96.
[52] H. Choi, S.R. Al-Abed, D.D. Dionysiou, E. Stathatos, P. Lianos, Sustainability science and engineering, in: I. Escobar, A. Schafer (Eds.), Sustainable Water for the Future, vol. 2, Elsevier Science, Netherlands, 2010, pp. 229–254.
[53] G.P. Anipsitakis, D.D. Dionysiou, Environ. Sci. Technol. 38 (2004) 3705–3712.
[54] P. Nfodzo, H. Choi, Chem. Eng. J. 174 (2011) 629–634.
[55] A. Fujishima, T.N. Rao, D.A. Tryk, J. Photochem. Photobiol. C. Rev. 1 (2000) 1–21.
[56] A.R. Khataee, M.B. Kasiri, J. Mol. Catal. A-Chem. 328 (2010) 8–26.
[57] S. Malato, J. Blanco, C. Richter, B. Braun, M.I. Maldonado, Appl. Catal. B: Environ. 17 (1998) 347–356.
[58] P. Nfodzo, H. Choi, Chem. Eng. J. 174 (2011) 629–634.
[59] A.A. Burbano, D.D. Dionysiou, M.T. Suidan, T.L. Richardson, Water Sci. Technol. 47 (2003) 165–171.
[60] A. Ajmal, I. Majeed, R.N. Malik, H. Idriss, M.A. Nadeem, RSC Adv. 4 (2014) 37003–37026.